

## **Notice of Violation of IEEE Publication Principles**

### **“Computational Model of Protein-Bound Uremic Toxins Kinetics During Hemodialysis and Dose Evaluation of Accurate Dialysis Using Deep Learning Techniques”**

by Jing Huang

in IEEE Access, April 2020

After careful and considered review of the content and authorship of this paper by a duly constituted expert committee, this paper has been found to be in violation of IEEE’s Publication Principles.

This paper has copied content from the papers cited below. The original content was copied with insufficient attribution (including appropriate references to the original author(s) and/or paper title).

### **“Removal of Protein-Bound Uremic Toxins during Hemodialysis Using a Binding Competitor”**

by Magdalena Madero, Karla B. Cano, Israel Campos, Xia Tao, Vaibhav Maheshwari, Jillian Brown, Beatriz Cornejo, Garry Handelman, Stephan Thijssen, and Peter Kotanko  
in Clinical Journal of the American Society of Nephrology, 14, 2019

### **“A Novel Mathematical Model of Protein-bound Uremic Toxin Kinetics during Hemodialysis”**

by Vaibhav Maheshwari, Stephan Thijssen, Xia Tao, Doris Fuertinger, Franz Kappel, Peter Kotanko  
in Scientific Reports, 7, 2017

Received March 30, 2020, accepted April 19, 2020, date of publication April 27, 2020, date of current version May 15, 2020.

Digital Object Identifier 10.1109/ACCESS.2020.2990725

# Computational Model of Protein-Bound Uremic Toxins Kinetics During Hemodialysis and Dose Evaluation of Accurate Dialysis Using Deep Learning Techniques

JING HUANG 

Department of Intensive Care Unit, Affiliated Cancer Hospital, Zhengzhou University, Zhengzhou 450000, China


e-mail: zlyyhuangjing1428@zzu.edu.cn)

**ABSTRACT** The protein-bound uremic toxins (PBUT), evolving to avoid conventional hemodialysis, decreases the toxin-free dissemination by a higher degree of binding of proteins, in turn increasing the dialyzer redirected membranes from it. Therefore, PBUT kinetics mechanical understanding can open ways of improving dialytic removal. A robust PBUT kinetic model has been developed, which consists of the various levels of compartment and dialyzer. This model represents a dynamic balance between protein, toxin and complex protein toxins. Further, this model has been calibrated and validated through literature, clinical evidence and studies is presented in this paper with numerical results. This anticipates key aspects of PBUT kinetic, which includes free and binding PBUT concentration profiles, where the dialytic variance PBUT has the elimination of dialysis rate effect. A popular Deep learning (DL) integrated PBUT kinetic model has been used in the elimination of non-dialysis dose evaluation conditions. The new DL-PBUT algorithm removes interruptions, helps to estimate the dialysis quality parameter (MR/Y), online with considerable precision with minimized delay and more efficiently than the known algorithms. The test results have been computed for various datasets which has been analyzed from the patients at lab scale shows promising outcomes.

**INDEX TERMS** Deep learning, uremic toxins, kinetic, complex protein toxins, clinical evidence.

## I. RELATED WORKS AND ITS BASIC STUDY

In the present era of research, three wide classes of Uremic toxins may be divided into: small, water-soluble and protein-free (MW) solutes  $< 300D$ ; median molecules ( $300 < MW < 12000D$ ); and protein-based molecular. The protein-bound uremic toxins include indoxyl sulphate (IS) (MW 251 D). IS is metabolized with indole liver, which is a tryptophan metabolite formed by intestinal flora [1]. It has been noticed that the level of serum in IS of chronic patients with kidney disease is significantly higher and speeds up chronic renal disease (CKD). In addition, studies indicate that IS increases the intake of oxygen and causes local hypoxia in renal tubular cells, and it can contribute to end-stage renal disease [2], [3]. It has shown that IS is capable to reactive oxygen species, endothelial dysfunction, and endothelial wound repair, which can contribute to cardiovascular disease

The associate editor coordinating the review of this manuscript and approving it for publication was Wei Wei .

and higher mortality among CKD patients. In the case of ERSD [4], the present dialysis method is mainly focused on the elimination of specific water-soluble compounds [5].

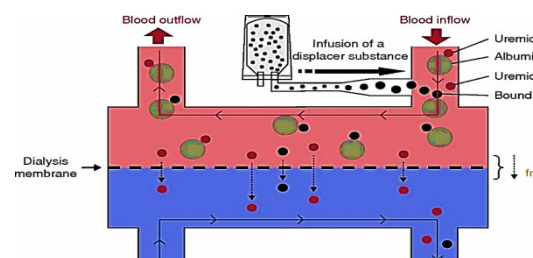


**FIGURE 1.** Uremic bounded toxin with infused substance.

As depicted in the Figure.1 [6] An artery (prefilter) blood-line is infused with a displacer in which the displacing molecule compete with the toxins that are protein-bound to binding places. This competition leads to higher free levels of toxin and to higher rates of toxin removal. PBUTs are

associated with a number of adverse reactions of patients with chronic kidney disease (CKD) and patients with end-stage renal disease (ESRD). In ESRD patients with hemodialysis (HD), a common report indicates that enhanced dialytic elimination [7], [8] would increase results for HD patients. Hence, PBUT removal is much lower than the elimination of non-protein-bound toxins in a standard high-flow HD. Therefore, the normal mode dialysis (NMD) has shown not to be substantially less than p-cresyl sulfate (pCS) or putative uremic toxins of indoxyl sulfate (IP). The problem is essentially hard where the protein association that reduces the direct dialysis fraction, so that the traditional high-flux HD (TH-FHD) only offers insufficient PBUT removal [9].

PBUTs are the most widely studied for all PCSs and IS, hence both of which are considered significant to this toxin class and both are more than 90% protein bound. In comparison with a height and weight-matched safe control point, pre-dialysis levels of the IS and pCS has been analyzed using 116 –and 41-fold, with unbound marker-toxins, urea and creatinine-level just 5 and 13-fold, respectively [10], [11]. In HD patients, physiological events, like cell dysfunction, oxidation stress, cell senescence, are causally associated both with IS and the pCS. It is directly associated with epithelial macrophages and increases atherosclerosis while PCS has endothelial dysfunction effects on semi-stimulated leukocytes and affects osteoblast cells by generating Reactive Oxygen Species (ROS). The normal IS & PCS reduction ratios are below 35% on high-flow HD, whereas for urea and creatinine more it shows more than 70% which are the same, that indicates the inefficiency in the eradication of conventional HDs [12]. Various methods have been studied, including hemodiafiltration, membrane absorption and competitive binding, in patients and studies to improve dialytic removal of PBUT [13], [14]. It is practically hard to compare all extracorporeal techniques with the appropriate power in human instances; in vitro studies, for example because of problems with emulsion quantities and liver metabolic rate, will be very challenging.

Increased blood volume, increased dialysis duration and the dialysis frequency, along with its flow and volume exchange rate coefficient beyond standard dialysis practice are the approaches to improving PBUT removal [15]. The addition of the convective hemodiafiltration structure only adds little more than the standard high flux of HD PBUT removal performance. Further, There are additional techniques for eliminating PBUTs, such as (i) toxin adsorption throughout dialysis on mixed-matrix membranes or adsorber zéolite silica, (ii) preservation of propagation gradient in albumin or activated carbon dialysis and (iii) displacement of PBUT by binding competitors, (iv) albumin toxins preference to use the high frequency electromagnetic field to increase the free toxin fraction;

In [16] authors reported a method for investigating the wavelength dependency between the ultraviolet (UV) absorbance in the spent dialysate and the remaining dissolved salts extracted during hemodialysis to clarify possibility for

estimating the optical dialysis suitability sensor for elimination of the dissolved salts. In the North-Estonian Regional Hospital's Department of Dialysis and Urology, 10 uremic patients are diagnosed with 30 hemodialysis therapies. However, the highest combination for urea, creatinine, potassium and phosphates used in dialyses was observed at wavelengths of 237 nm which were new developments compared to previous studies. The highest combination of UV absorption and uric acid in spent dialysate was observed at a wavelength of 294 nm. A selectiveness for several compounds can be achieved by getting at least two separate wavelength regions.

Heart problems also arise in patients with kidney failure [17] as shown in the Figure.2. as inferred from health Harvard datasets.

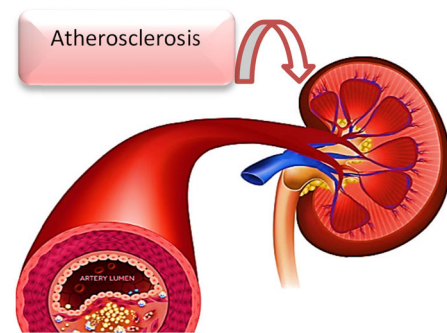


FIGURE 2. Heart disease with kidney failure.

The reported model has been upgraded to reflect the known effects of uremia on a large number of ionic formations to provide the conceptualization for cardiovascular cellular reactivity effects from uremia leads to Artherosclerosis. The model was used to study the effects on duration of action potential (APD) of uremia and of dialyses therapy in reaction to the S1-S2 protocol for this renal artery stenosis. The uremic myocyte was found to be a modified temporary repolarization and a short APD. The uremic myocyte was found to have an enhanced transient re-polarization and a decreased APD. Uremia also affected APD recovery. The action potential acquired after short diastolic intervals at the end of dialysis was distinguished by the absence of the stage of the plateau.

Author introduced a study to determine whether the ventricular premature beats (VPBs) in peripheral blood volume variability are significantly linked in the course of dialysis treatment to hypotensive symptoms mathematical approach (HSMA) [18]. Patients receiving hemodialysis often suffer from cardiovascular disorders and uremic neuropathy, which in turn leads to intradialytic hypotension, cramps, nausea, dizziness, headaches and other complications. VPBs, which are common in patients receiving hemodialysis, can be seen as internal disturbance causing equilibrium by severe drop in blood pressure and sustained tissue deoxygenation. This analysis explores the relative volume changes from fingertips photo plethysmography and their relevance to characterizing the physiological recovery of an altered circulatory state caused by VPB and quantifies it.

The regeneration unit for dialysates is an important part of the portable artificial renal, where its principal purpose being to purify dialysates from uremic contaminants, to regulate pH, to correct the electrolyte concentration and osmotic concentration [19], [20]. Here, authors proposed to combine sorbent and electrochemical techniques for dialysis regeneration. The procedure was carried out in chronic kidney disease patients on spent dialytic samples. The experiment regulated the substrates of nitrogen and the electrolytes. The dialysis solution has been regenerated for dialysis regeneration unit efficiency testing. The implemented dialytic regeneration unit can potentially be used in artificial wearable kidneys, whereas further animal testing is necessary for the device.

**II. MATERIALS AND METHODS**

**A. MATHEMATICAL MODEL FOR PBUT KINETICS**

The developed multi-compartment deep learning model of the patient and the PBUT dialyzer model, has been used for describing PBUT kinetics. The 2-compartment approach has been used to analyze urea kinetics and estimate the parameter.

**B. DEEP LEARNING BASED PATIENT MODEL**

A detailed learning two-part model is developed for patients consisting of a plasma, interstitial and intracellular compartment with a plasma and interstitial protein-bound fraction and free fraction in each compartment.

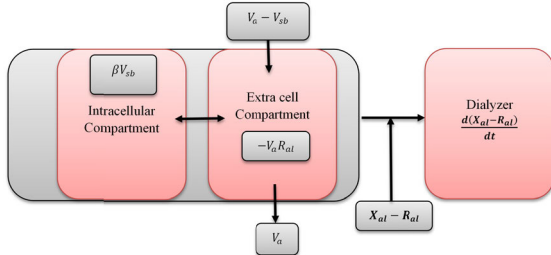


**FIGURE 3. Two part dialyzer model.**

Figure.3. shows a block diagram in which the dialyzer is followed by a three-compartment illustration of the patient. The toxic blood is stored in the patients and the dialyzer is squeezed. The free toxin in the dialyzer propagates to the dialyzer from the blood. The ultra-filtered fluid often releases a small fraction of the free toxin. The patient gets the 'clean' blood after the downstream dialyzer, and the procedure in traditional HD configuration takes 4 hours.

Compared with other kinetic PBUT models that depend on the overall toxic intensity difference (free and bound) in interchangeable diffusion, the model proposed is stronger when only free toxin is exchanged between plasma and the interstitial region. Albumin is not supposed to be exchanged in plasma for interstitial compartments with the albumin complex. Plasma pool for dialytic toxins is the diffusive transfer from an interstitial pool to an interstitial pool of the free fragment and the transfer of toxins from IC to an interstitial pool. Reduced rates of free toxins also dissociate the complex

of protein-toxins from the plasma and interstitial pools in each portion. Further albumin distribution is estimated to be almost 40% of all the albumin mass and 60% to the interstitial pool, respectively, in HD patients. The interstitial flow rate, however, is significantly higher than that of plasma, and is significantly lower than that of plasma albumin. The plasma compartment is equal as the mass balance of toxins in the presented model.

Accumulation rate of toxins

$$\begin{aligned}
 &= \text{Plasma compartment leaving toxin}(V_a) \\
 &+ \text{Plasma compartment entering the toxin with } (V_a - V_{sb}) \\
 &+ \text{Diffusive mass transmission from space} \\
 &+ \text{Convective mass movement from space} \\
 &+ \text{Conditions for reaction rate based on kineti} \quad (1)
 \end{aligned}$$

where  $V_a$  and  $V_{sb}$  are both plasma flow and ultrafiltration rate. Equation (2,3&4) indicates the resulting mass balance equations in the plasma compare with free toxin, complex protein-toxin, and free protein. The law governs the kinetic reaction of complex protein toxins.

$$\begin{aligned}
 \frac{d(X_{al} - R_{al})}{dt} &= -V_a R_{al} + (V_a - V_{sb}) R_{out} \\
 &+ M_{ja,R} (R_{bq} - R_{al}) + \beta(-m_1 A_{al} R_{al} \\
 &+ m_2 A_{al}) X_{al} \quad (2)
 \end{aligned}$$

$$\begin{aligned}
 \frac{d(X_{al} - A_{al})}{dt} &= -V_a A_{al} + (V_a - V_{sb}) A R_{out} \\
 &+ (m_1 A_{al} R_{al} + m_2 A R_{al}) X_{al} \quad (3)
 \end{aligned}$$

$$\begin{aligned}
 \frac{d(X_{al} - A R_{al})}{dt} &= -V_a A R_{al} + (V_a - V_{sb}) A_{out} \\
 &+ (m_1 A_{al} R_{al} + m_2 A R_{al}) X_{al} \quad (4)
 \end{aligned}$$

Equation (5,6 & 7) provides mass balance in an interstitial compartment for free toxins, protein-toxin complex and free protein;

$$\begin{aligned}
 \frac{d(X_{jw} - R_{jw})}{dt} &= M_{jd} (R_{jd} - R_{jw}) - M_{ja,R} (R_{bq} - R_{al}) \\
 &- \beta V_{sb} R_{jw} + (-m_1 A_{jw} R_{jw} + m_2 A R_{jw}) X_{jw} \quad (5)
 \end{aligned}$$

$$\frac{d(X_{jw} - A R_{jw})}{dt} = (m_1 A_{jw} R_{jw} - m_2 A R_{jw}) X_{jw} \quad (6)$$

$$\frac{d(X_{jw} - A_{jw})}{dt} = (-m_1 A_{jw} R_{jw} + m_2 A R_{jw}) X_{jw} \quad (7)$$

The equation (8) provides a free toxin equilibrium between the weight of an intracellular compartment when toxin production will occur at a consent rate and created toxins are diffused into the interstitial body at levels of concentration.

$$\frac{d(X_{jw} - A_{jw})}{dt} = H - M_{jd,R} (R_{jd} - R_{jw}) \quad (8)$$

A patient loses a considerable quantity of fluid during dialysis based in the urea transponder as shown in the Figure.4.

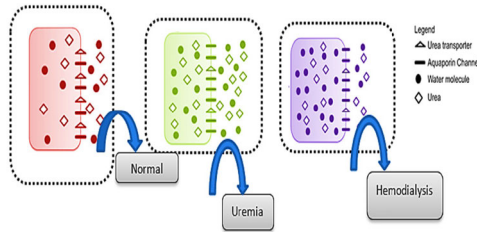


FIGURE 4. Fluid dialysis.

Fluid is expected to be collected at the constant ultrafiltration rate ( $V_{sb}$ ) and ultrafiltration fluid removal is proportional to the volume in the compartment. During dialysis, intracellular fluid volume as measured by multi-frequency biomass is assumed to be normal. Unknown sample parameters in the model are the initial compartment quantities, and toxin concentrations are estimated. The plasma compartment Fluid Balance is defined as,

$$\begin{aligned} & \text{Rate of plasma volume change} \\ &= \text{Fluid that leaves the person } (-V_a) \\ &+ \text{Fluid that enters the patient } (V_a - V_{sb}) \\ &+ \text{Fluid flows from under interstitial areas } (\beta V_{sb}) \quad (9) \end{aligned}$$

Equation (5) is provided for time-sensitive variations in plasmas and the interstitial fluid volumes.

$$\frac{d(R_{al})}{dt} = -(1 - \beta)V_{sb} \quad (10)$$

$$\frac{d(R_{jw})}{dt} = -\beta V_{sb} \quad \text{where } \beta = \frac{R_{jw}}{R_{jw} + R_{al}} \quad (11)$$

In Equations (2-11),  $R_{jw}$ ,  $R_{al}$ ,  $R_{jw}$ , indicates free plasma toxin concentration ( $al$ ), interstitial toxin and concentration ( $jd$ );  $R_{al}$ ,  $R_{jw}$ ,  $R_{jd}$ , shows the corresponding compartmental fluid volumes;  $A_{al}$ , and  $A_{jw}$ , are protein-toxin complex volume concentrations;  $A_{al}$ ,  $A_{jw}$  free plasma protein and interstitial compartment concentration.

A protein toxin binding site is assumed for the current model. In addition, most PBUTs have more than one albumin molecule site. It also connects a small secondary site but most of the IS connects to a primary highly affinity site.

However, the model developed does not take into consideration the competition between PBUTs. This means that each PBUT interacts separately on the plasma and interstitial pool and the dialyzer with the albumin molecule.

### C. MODEL OF DIALYZER

The flow of blood / plasma testing is counter-actual. Blood dialysis diffuses freely on the side, causing protein complex dissociation and blood side free toxin. The definition of standard dialyzer clearance (MS) therefore cannot explain the complex PBUT dynamics and is characterized by the inlet and exit concentrations of the dialyzer and is represented for uric solutes which are nonprotein-based. For calculating diffusive mass transfer via hollow fibers, the membrane mass

transfer coefficient ( $M_oB$ ) of the above model is used.  $M_oB$  is a membrane property that is relatively constant but still less than 500 db based on the molecular weights of the toxin. In this analysis the fiber-based dialysis and blood fluid in PBUTs are considerably smaller (175-284 gr/mol) and all PBUTs are required to show the same  $M_oB$ .

### D. MODEL OF BLOOD SIDE

Equation (12) demonstrates a space-time representation of blood side toxin levels, protein / toxin complex, and free protein.

$$\begin{aligned} \frac{\partial R}{\partial r} &= -\frac{1}{NA} \frac{\partial}{\partial y} (V_a R) - \frac{1}{NAL} (M_oB (R - R_e) \\ &+ V_{sb} \bar{R}) + (-m_1 A \cdot R + m_2 AR) \quad (12) \end{aligned}$$

$$\frac{\partial AR}{\partial r} = -\frac{1}{NA} \frac{\partial}{\partial y} (V_a AR) + (-m_1 A \cdot R + m_2 AR) \quad (13)$$

$$\frac{\partial A}{\partial r} = -\frac{1}{NA} \frac{\partial}{\partial y} (V_a A) + (-m_1 A \cdot R + m_2 AR) \quad (14)$$

Equation (12-14) initial and limit conditions are:

$$C_a(y) | r = 0 = 0;$$

$$C_a(y) | y = 0, \text{ Patient plasma concentration}$$

where  $C = R$  or  $C = AR$  or  $C = A$

Here,  $(M_oB (R - R_e) + V_{sb} \bar{R})$  indicates the blood to the dialysis side by diffusive and convective toxin transfer. All diffusion and convection eliminate toxins in the dialyzer. There are no identical diffuse and convective effects, because increased convection decreases the blood-free concentration, causes the diffuse gradient to be smaller and vice versa. The Péclet number  $Pn = \frac{V_{sb}}{M_oB}$  is used to change the convective flux in the event of a diffuse flux for the diffusive and convective volume. In this case,  $R$  indicates the free toxin concentration within the membrane which contributes to convective flow. It is the function of both free plasma  $R$  and dialysate  $R_e$ ,  $\bar{R} = \frac{1}{A_e} - \frac{1}{d^{A_e-1}}$ . In view of a uniform and equal flow of blood across every fiber it could be stated that  $\frac{M_oB}{F}$ , where  $F$  is the total number of fibers, is a propagating removal by an individual fiber.

In the dialyzer, the fiber length decreases due to ultrafiltration with regard to the plasma flow rate ( $V_a$ ).  $V_a$  has been assumed to decrease linearly along the length of the fiber (Equation (15)).

$$V_a(y) = V_{aj} - \frac{y}{L} V_{sb} \quad (15)$$

In this case,  $V_a(y)$  is a flow rate of plasma in the fiber soluble;  $B$  is an inner component of the blood fiber. Because of the lower axial diffusion coefficient in blood resolution, the axial diffusion of the fiber length is ignored. This is similar to the presumption of a connection flow and the mass transmission between adjacent connectors is not available.

### E. MODEL OF DIALYSATE SIDE

Dialysate loops around each fiber throughout the annulus space. The flow of dialysates is expected to be compatible

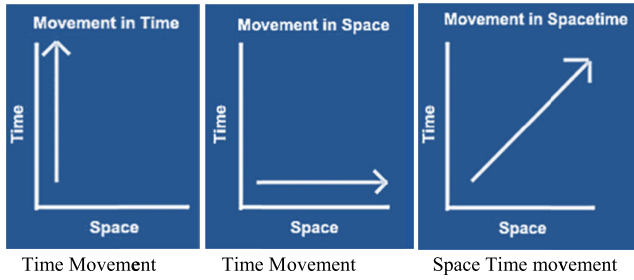


FIGURE 5. Space Time analysis for blood side toxin.

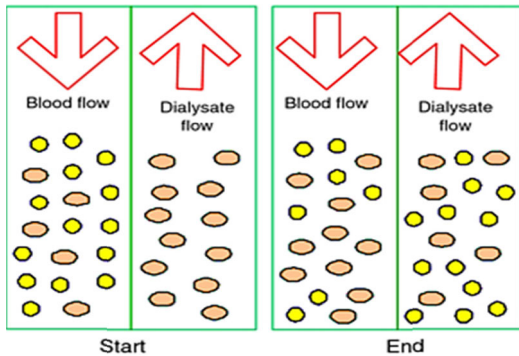


FIGURE 6. Blood flow vs dialysate flow.

and also shared between the N fibers in the dialyzer. The spatiotemporal descriptions of the concentration in the dialysate flow boundary is presented in figure.6 are given in Equation (16), similar to the blood side model.

$$\frac{\partial R_e}{\partial r} = -\frac{1}{NA_e} \frac{\partial}{\partial y} (V_e R_e) + \frac{1}{NA_e L} (M_o B (R - R_e) + V_{sb} \bar{R}) + V_{sb} \bar{R} \quad (16)$$

In this case, the  $A_e$  is the dialysate flow area in the range of the single fiber. If  $C_g$  is the diameter of the dialyzer containing N Fiber,  $r_b$  is the internal radius of the fiber,  $x_b$  is the thickness of the fiber.

In this case, the  $A_e$  is the flow dialysate in the fiber set. Where  $C_g$  diameter is the N-fiber dialyzer,  $r_b$  is the internal fiber length,  $x_b$  is the fiber thickness.

$$A_e = \frac{\pi C_g^2}{4N} - \pi (r_b + x_b)^2 \quad (17)$$

The flow of dialysate is also increased by ultrafiltration, as shown in the equation (18), by the fluid that has been removed from the blood side of dialysis.

$$V_e(y) = V_{ej} + \frac{L - y}{L} V_{sb} \quad (18)$$

Here  $V_{ej}$  is the dialytic flow inlet,  $L$  the fiber length and  $y$  the fiber axial position. The dialytic (Equation (16)) model is considered to be free only toxin, as no dialytic protein or protein-toxin complex exists.

$$R_e(y) | r = 0 = 0; \\ R_e(r) | y = L = 0;$$

The blood-side transition of toxin to dialysate side has 3 resistances:

- The boundary layer of the blood side,
- The resistance to the hollow membrane fiber and
- The dialysate boundary layer. The membrane transmission coefficient ( $M_o B$ ) membrane resistance substitution lumps together all three resistances in this article model. ( $M_o B$  is also assumed to remain constant during dialysis, i.e. that there is no changes in blood circulation and dialysis.

F. ESTIMATION OF DIALYSIS DOSE

Differential equations describing urea mass during dialysis presume that fixed volume, single kinetic pool in urea elimination, consider the rate of production of urea, ultra-filtration and rebound is negligible, with the dialysis quality parameter  $MR/Y$  as calculated, that the  $M/Y$  ration remains consistent as shown in the graphical analogy as shown in the Figure7.

$$\frac{MR}{Y} = -\ln \frac{B_r}{B_o} \quad (19)$$

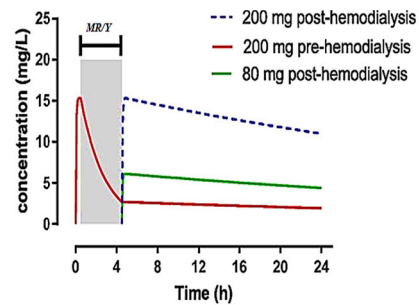


FIGURE 7. Estimation of dialysis dose.

where the concentrations of  $B_r$  and  $B_0$  are blood urea prior to the beginning of the procedure, and where they are at a given time(h) during the ongoing dialysis process with respect to various milli gram (mg) level concentration. At a certain point in the ongoing dialysis ( $Z_r$  and  $Z_0$ ), the UV absorbance maximal value was used to determine the spectrophotometric dialysis dose of  $MR/Yz$ , not the urea concentration before and after dialysis.

$$\frac{MR}{Yz} = -\ln \frac{Z_r}{Z_o} \quad (20)$$

In accordance with the Daugirdas second-generation formula, single pool volume  $\frac{MR}{Y}$  for  $\frac{psMR}{Yx}$  Blood, taking into account urea generation and ultrafiltration.

$$\frac{psMR}{Yx} = -\ln \left( \frac{B_{end}}{B_0} - 0.008 \frac{R}{60} \right) + \left( 4 - 3.5 \frac{B_{end}}{B_0} \right) \frac{RW}{X} \quad (21)$$

where  $B_{end}$  is the concentration of end-dialysis,  $R$  is the dialysis length,  $RW$  it is the total ultrafiltration kilogram and  $X$  is the dry body weight of the patient is in kilogram.

The mono-compartmental equation (21) can be defined in UV values.

$$\frac{psMR}{Y_z} = -\ln\left(\frac{Z_{end}}{Z_0} - 0.008\frac{R}{60}\right) + \left(4 - 3.5\frac{Z_{end}}{Z_0}\right)\frac{RW}{X} \quad (22)$$

where at the end of dialysis  $Z_{end}$  is UV absorbance. The balanced  $\frac{MR}{Y}$ ,  $\frac{eMR}{Y}$ , Dialysis Rate ( $\frac{MR}{Y}$ ) is predicted by adjustment rate based on multi-compartmental effects of urea removal during dialysis.

$$\frac{eMR}{Y} = \frac{psMR}{Y} - \left(\frac{R}{60}\right)\frac{psMR}{Y} + 0.03 \quad (23)$$

The speed adjustment method predicts that the rebound urea is associated with dialysis or dialysis rates.

As a result of validation of an independent and accurate  $\frac{MR}{Y}$  estimation algorithm in comparison to a previous study, feedback from the dialysis machine (for example, blood changes or dialysate flow).

### G. ALGORITHM FOR EVALUATION AND ANALYSIS

A new deep learning algorithm, consisting of average signals and signal increment frequency, is thus suggested for online measurement of them by using calculated UV absorbance data. At the same time, the new algorithm helps solve difficulties if a raw UV absorption signal causes noise and credibility disorders.

Two principles of Deep Learning signal processing are brought together to achieve speed and accuracy of the calculations: the Average procedure applies linear accessories of the measured data to achieve higher calculation speeds while the signal increment frequency procedure continuously collects incremental raw data that restores online the  $\frac{MR}{Y}$  curve characteristics.

### H. AVERAGE PROCEDURE

Average main ideas include: (1) ignore the measured signals if the noise reaches the acceptable level; and (2) take into consideration as far as possible of the average increase in metrics.

The procedure, in the latter case, matches the measured signals linearly. The problem may be minimized when the curve is placed into small windows of determined signals, since the exponential behavior of  $\frac{MR}{Y}$  is not included. The simple fit algorithm measures signal in real time and can therefore be expected to progress in dialysis.

The  $n(r)$  calculation depends on the stability of the signal  $s(r)$ , i.e. whether or not that we have defined time as a CP.

$$n(r) = \begin{cases} n(r-1) + \frac{sum}{r}, & \text{if } n(r-1) + \frac{sum}{r} < s(r) \\ s(r), & \text{otherwise} \end{cases} \quad (24)$$

If the measured signal is not stable in current moment  $r$  (this is not a CP), the measured value will first be calculated

as  $s*(r) = average * r$

$$n(r) = \begin{cases} n(r-1) + average, & \text{if } n(r-1) + average < s*(r) \\ s*(r), & \text{otherwise} \end{cases} \quad (25)$$

If the raw signal stops growing, and a value greater than that measure the red, i.e.  $n(r) > s(r)$ , and  $n(r) = n(r-1)$  remains the value of the measured signal.

### I. SIGNAL INCREMENT FREQUENCY PROCEDURE

The average for smoothing and monitoring of the highest peaks is accurate. The determined curve may not be monotonous, but cannot be used in this entire event to measure the duration of the dialysis cycle in order to decide whether or not the mechanism should be supported in the process. The proposed signal increase frequency process which provides a better way to forecast the behavior of the process.

In Signal Increment Frequency, the idea is often used to diagnose digital circuit faults, when the frequency of effects on test systems determines suspected applicant faults.

The frequencies of different signal increments  $\Delta(r) = n(r) - n(r-1)$  are calculated to implement this idea for estimating the  $\frac{MR}{Y}$  curve growth. Consequently, histograms as in Figure.8.(a) for every moment are received [21].

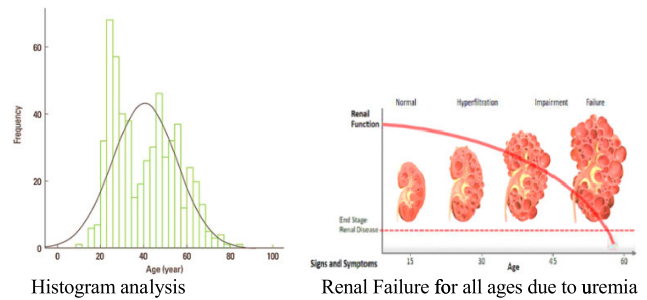


FIGURE 8. Histograms analysis for various ages.

At each moment, the  $\frac{MR}{Y}$  curve calculation can be done by an increment with the maximum value i.e.  $\Delta_{max}$ . From the Figure.7. histograms can be concluded with the following [22], [23].

1. It can see that the measured signal increments are rather unreliable, due to the many “competitive” increments with respect to age as shown in the Figure.8(b).
2. If there is no clear increment from the others, it is impossible to select a major increment that best estimates the value of  $\frac{MR}{Y}$  on the basis of the data obtained from the raw signals.

The average over a subset of  $n$  largest increments in window  $L$  to eliminate the effect of such an inherent noise in histograms is quantifiable. The calculations can be performed as follows:

$$n(r) = n(r-1) + \frac{1}{m} \sum_{j=1}^m \Delta_j \quad (26)$$

However, the signal increment frequency algorithm will be identical to Average when it includes the entire histogram in L at extreme case. Therefore, the size of window L should be carefully selected to ensure the estimation of the progress of the dialysis cycle is accurate enough. The window size L has been calculated for every session based on a pre-analysis of the treatments observed. To consider the exponential behavior of  $\frac{MR}{Y}$ , calculations can be enhanced through the use of dynamic histograms that are measured using a continuously changing time window with a constant duration for the whole cycle.

Note that the signal increase frequency algorithm associates a certain delay. The collection of statistics will take time to predict the behavior of the process with great confidence. The average works better at the start of the process. The signal increase frequency algorithm, on the other hand, is more monotonous than Average which helps to predict better if appropriate statistic is obtained.

1) DEEP LEARNING COMPUTATION

Deep Learning [24] combines Average and signal increment frequency positive characteristics [25]. While Average increases measured decision stability, signal increment frequency enhances Average curve in the states where the raw signal loses credibility by beginning to fall rather than grow.

The equations in Deep Learning in the CPs are as follows:

$$n(r) = \begin{cases} s(r), & \text{if } n(r-1) + \frac{\text{sum}}{r} < s(r) \\ n(r-1) + 1, & \text{otherwise} \end{cases} \quad (27)$$

Outside the CPs, then calculate

$$n(r) = \begin{cases} n(r-1) + \text{Average}, & \text{if } n(r-1) + \text{average} < s*(r) \\ n(r-1) + \frac{1}{m} \sum_{j=1}^m \Delta_j, & \text{otherwise} \end{cases} \quad (28)$$

For the purpose of the smoothing of the  $\frac{MR}{Y}$  curve and extrapolation, the signal increment frequency in the Deep Learning algorithm is implemented in average for the estimation of the curve between CPs.

III. RESULTS AND DISCUSSION

A. DIALYSIS ESTIMATION RESULTS

The results of clinical and modeling demonstrate that Deep learning assisted signal processing [26] has significant positive effects on on-line data visualization as shown in the Figure. 9. The readability of all algorithms and the dialysis calculation are greatly improved. The algorithms function properly in many cases and avoid the raw signal curve. The estimated UV dose is similar to that of the blood urea calculated as  $eMR/Y$ , which following the application of a deep learning algorithm is closest to  $eMR/Y$ . The estimated dose is similar with the UV method. Further, for experimental analysis the datasets has been taken from <https://www.ncbi.nlm.nih.gov/>

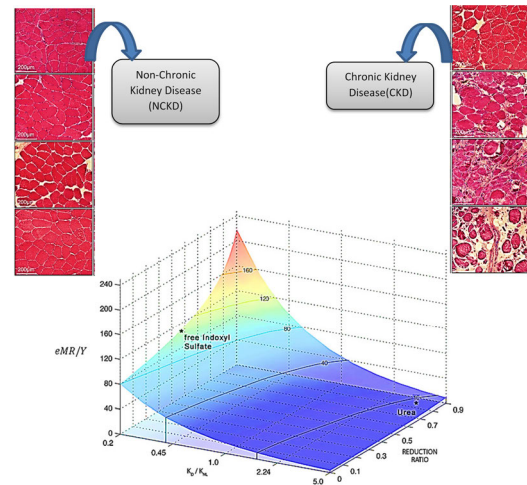


FIGURE 9. On-line data visualization for NCKD vs CKD.

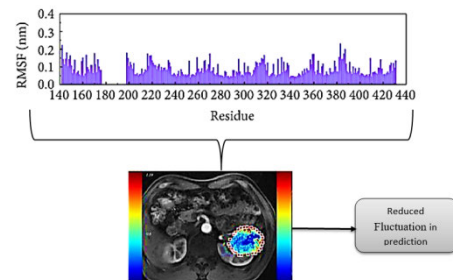


FIGURE 10. RMSF analysis.

This is confirmed by previous studies where UV measured dialysis results are comparable to those of the blood urea calculated for the dialytic clearance to normal kidney as shown in the Figure.9. The real-time dose calculation is similar to the blood comparison, as the lower RMSE value, using the algorithms than the raw UV-absorption signal. Nevertheless, the drawback of this analysis is the calculations for  $\frac{eMR}{Y}$  and Root mean square Fluctuation (RMSF) as shown in the Figure.10.have been based on two blood-urea-point measurements, supposed to take the single-pool removal rule, which is often violated, Hence it cannot accurately reflect the true behavior of the blood uremic solute. Further regular blood tests can be avoided, which might be troublesome because of the risk of anemia in dialysis patients. Additionally, a single-pool removal behavior, approximate calculation of the degree of violation can be assessed by measuring the rebound effect.

If raw signal variations occur exceptionally,  $\frac{MR}{Y}$  is more accurately monitored by the deep learning algorithm than by the other algorithm This is because of an option for signal tuning which has been used in Deep learning (DL) integrated PBUT kinetic model during evaluation conditions which has been represented in the Figure.11.clearly for kidney tissue with high uremia composition, which easily brings the computer curve closer to raw curve and prevents abrupt changes through the use of raw signal growth away from the average signal growth.



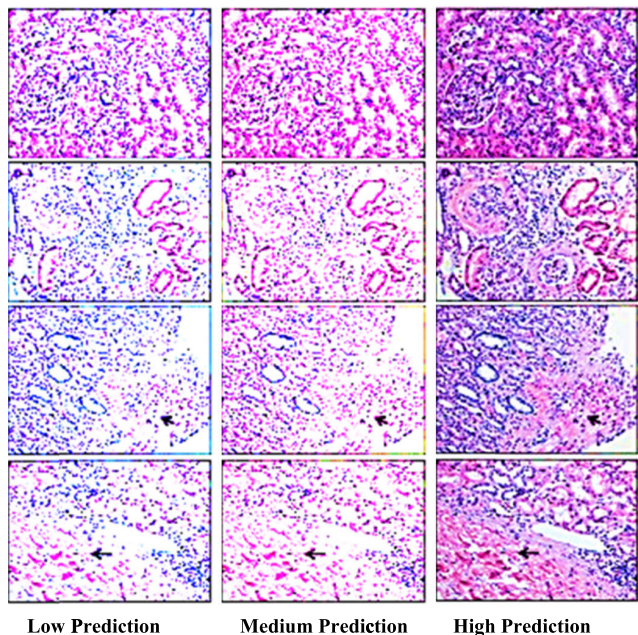


FIGURE 11. Signal tuning for fine image analysis.

TABLE 1. Numerical prediction analysis.

Total Available Patient Dataset	NMD	UV	HSMA	TH-FHD	HD	DL-PBUT
10	77.1	77.7	77.4	79.9	79.7	70.3
20	47.7	57.7	79.3	79.9	84.9	87.3
30	70.9	71.1	79.9	79.9	87.4	89.9
40	77.3	79.3	83.7	87.3	89.9	97.9
50	74.9	89.7	90.9	91.9	94.9	97.7
60	77.2	87.4	91.8	92.4	93.4	96.9
70	77.3	87.3	89.3	90.3	91.9	97.11
80	79.3	80.7	89.7	90.7	92.7	97.9
90	79.7	80.4	81.7	90.7	93.9	97.9
100	74.7	87.9	88.1	90.7	93.7	97.8

Furthermore, when the raw signal varies from its expected behavior, normally after drastic rising or dropping raw signal, a better prediction of process prolongation can be made from the deep learning algorithm with numerical data as shown in the table.1. In the future, the algorithm of deep learning needs to be better adapted to a broad set of data, in which the characteristics can be further evaluated and linked with real clinical data.

**B. PREDICTION OF THE MODEL**

The optimized model has been used to describe the distribution across all PBUTs. Figure.12.(a) presents the corresponding results for the scaling factor for blood

TABLE 2. Validation based on performance analysis.

Total Available Patient Dataset	NMD	UV	HSMA	TH-FHD	HD	DL-PBUT
10	66.1	66.7	67.4	68.8	69.6	60.3
20	46.6	46.6	68.3	68.8	64.9	66.3
30	60.8	61.1	68.9	73.8	77.4	79.8
40	66.3	69.3	73.6	89.3	86.8	86.9
50	84.9	88.7	89.8	90.9	83.8	97.6
60	84.3	87.4	88.6	89.4	80.4	90.9
70	66.3	67.3	68.3	69.3	76.8	89.11
80	69.3	60.6	68.6	63.6	74.6	86.8
90	79.6	80.4	81.6	88.6	88.8	89.9
100	84.6	86.8	86.1	90.7	88.7	98.1

circulation analysis. Note that the unequal distribution of molar toxins in plasma and interstitial body parts due to the disparate albumin distribution has been clearly demonstrated by this concentration of PBUT.

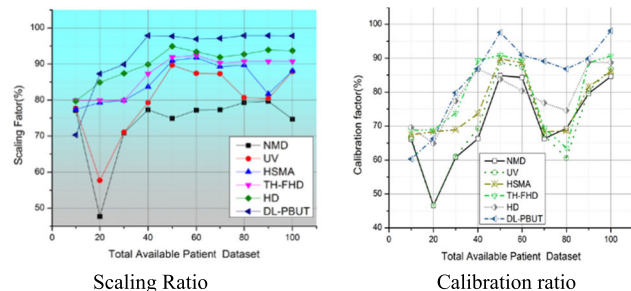


FIGURE 12. Scaling factor Vs Calibration analysis.

Scaling factor also makes it possible to compare PBUTs side by side. In order to assess the effect of increased blood fluid and dialysis, a modified model has been employed. The results show high calibration process which has taken on dialysis and individual parameters of toxins as shown in Figure.12(b).

**C. VALIDATION OF THE MODEL**

The initial PBUT concentrations for model simulation have been used as a test to detect model performance against these in results from the model calibration stage as shown in the table.2. For these simulations, the model parameters found during the experiment have been used. The model performance has been tested in the areas as described, Furthermore, it is impossible to assess if the simulated knowledge is related to the experimental data on a separate level in both first regions. The original level of binding of protein is unique to the 10 patients class of patients. Hence based on the

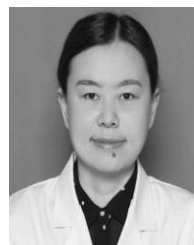
experimental results, datasets which has been analyzed from the patients at lab scale shows promising outcomes.

#### IV. CONCLUSION AND FUTURE EXTENSION

In this paper kinetic PBUT models that depend on the overall toxic intensity difference in interchangeable diffusion, hence this model has been proposed for free toxin which is exchanged between plasma and the interstitial region. Therefore, Deep learning (DL) integrated PBUT kinetic model has been used in the elimination of non-dialysis dose evaluation conditions. The new DL-PBUT algorithm removes interruptions, helps to estimate the dialysis quality parameter ( $\frac{MR}{Y}$ ). Further, the Differential equations describing urea mass during dialysis presume the fixed volume, where the single kinetic pool in urea elimination, consider the rate of production of urea, ultra-filtration and rebound is negligible, with the dialysis quality parameter  $MR/Y$  based on experimental validation based on NCKD and CKD analysis. In future. Advanced deep assisted neural concepts has been planned to hybridize to improve the prediction rate.

#### REFERENCES

- [1] F. Uhlin and I. Fridolin, "Optical monitoring of dialysis dose," in *Modeling and Control of Dialysis Systems*. Berlin, Germany: Springer, 2013, pp. 867–928.
- [2] A. Ghanifar and V. R. Nafisi, "Optimal wavelength selection in ultraviolet spectroscopy for the estimation of toxin reduction ratio during hemodialysis," *Iranian J. Med. Phys.*, vol. 13, no. 2, pp. 77–85, 2016.
- [3] L. Possenti, G. Casagrande, M. L. Costantino, and P. Zunino, "Numerical modelling of microcirculation fluid exchanges in uremic patients accounting for the non-linear effect of lymphatic system," Politecnico di Milano, Milan, Italy, Tech. Rep. 35/2018, 2017.
- [4] G. Casagrande, L. Possenti, and M. L. Costantino, "Modelling of cardiovascular alterations during CKD progression," *Int. J. Artif. Organs*, 2017.
- [5] C. J. Sperati, "Hemodialysis: Initiation and complications," in *Clinical Decisions in Nephrology, Hypertension and Kidney Transplantation*. New York, NY, USA: Springer, pp. 333–348, 2013.
- [6] F. D. Gaetano, M. Serrani, J. Brubert, J. Stasiak, G. Moggridge, and M. L. Costantino, "Injection moulding process: CFD evaluation on the orientation of polymeric chains for manufacturing heart valves," in *Proc. Eur. Soc. Artif. Organs*, 2015, p. 389.
- [7] K. L. Saum, "Targeting endothelial Kruppel-like factor 2 (KLF2) in arteriovenous fistula maturation failure," Ph.D. dissertation, Dept. Eng. Appl. Sci., Biomed. Eng., Univ. Cincinnati, Cincinnati, OH, USA, 2018.
- [8] B. K. Birmingham, S. K. Swan, T. Puchalski, P. Mitchell, C. Azumaya, J. Zalikowski, and Y. Wang, "Pharmacokinetic and pharmacodynamic profile of rosuvastatin in patients with end-stage renal disease on chronic haemodialysis," *Clin. Drug Invest.*, vol. 33, no. 4, pp. 233–241, Apr. 2013.
- [9] S. Eloot, D. Schmeditz, T. Cornelis, W. Van Biesen, G. Glorieux, A. Dhondt, J. Kooman, and R. Vanholder, "Protein-bound uremic toxin profiling as a tool to optimize hemodialysis," *PLoS ONE*, vol. 11, no. 1, 2016, Art. no. e0147159.
- [10] N. Neiryneck, R. Vanholder, E. Schepers, S. Eloot, A. Pletinck, and G. Glorieux, "An update on uremic toxins," *Int. Urol. Nephrol.*, vol. 45, no. 1, pp. 139–150, 2013.
- [11] L. Viaene, P. Annaert, H. de Loor, R. Poesen, P. Evenepoel, and B. Meijers, "Albumin is the main plasma binding protein for indoxyl sulfate and p-cresyl sulfate," *Biopharmaceutics Drug Disposition*, vol. 34, no. 3, pp. 165–175, Apr. 2013.
- [12] O. Deltombe, B. W. Van, G. Glorieux, Z. Massy, A. Dhondt, and S. Eloot, "Exploring protein binding of uremic toxins in patients with different stages of chronic kidney disease and during hemodialysis," *Toxins*, vol. 7, no. 10, pp. 3933–3946, 2015.
- [13] R. Vanholder, G. Glorieux, and S. Eloot, "Once upon a time in dialysis: The last days of  $Kt/V$ ?" *Kidney Int.*, vol. 88, no. 3, pp. 460–465, Sep. 2015.
- [14] F. Brettschneider, M. Tölle, M. von der Giet, J. Passlick-Deetjen, S. Steppan, M. Peter, V. Jankowski, A. Krause, S. Kühne, W. Zidek, and J. Jankowski, "Removal of protein-bound, hydrophobic uremic toxins by a combined fractionated plasma separation and adsorption technique," *Artif. Organs*, vol. 37, no. 4, pp. 409–416, Apr. 2013.
- [15] M. Madero, K. B. Cano, I. T. X. Campos, V. Maheshwari, J. Brown, and P. Kotanko, "Removal of protein-bound uremic toxins during hemodialysis using a binding competitor," *Clin. J. Amer. Soc. Nephrol.*, vol. 14, no. 3, pp. 394–402, 2019.
- [16] J. Jerotkskaja, K. Lauri, R. Tanner, M. Luman, and I. Fridolin, "Optical dialysis adequacy sensor: Wavelength dependence of the ultra violet absorbance in the spent dialysate to the removed solutes," in *Proc. 29th Annu. Int. Conf. IEEE Eng. Med. Biol. Soc.*, Aug. 2007, pp. 2960–2963.
- [17] G. Callisesi, C. Corsi, and S. Severi, "Computational analysis of uremia effects on ventricular action potential," in *Proc. Comput. Cardiology*, Sep. 2008, pp. 1021–1024.
- [18] E. Grigonytė, E. Gil, P. Laguna, and L. Sörmö, "Relative peripheral blood volume changes in response to ventricular premature beats during dialysis," in *Proc. Comput. Cardiol.*, Sep. 2013, pp. 209–212.
- [19] B. M. Putrya, N. M. Zhilo, A. V. Baklanova, and N. A. Bazaev, "In vitro experiments of dialysate regeneration unit on waste dialysis fluid," in *Proc. IEEE Conf. Russian Young Researchers Electr. Electron. Eng. (EICoRus)*, Jan. 2019, pp. 2286–2289.
- [20] X. Tao, S. Thijssen, P. Kotanko, C.-H. Ho, M. Henrie, E. Stroup, and G. Handelman, "Improved dialytic removal of protein-bound uraemic toxins with use of albumin binding competitors: An in vitro human whole blood study," *Sci. Rep.*, vol. 6, no. 1, pp. 1–9, Sep. 2016.
- [21] X. Wang, Y. Zhang, X. Ren, Y. Zhang, M. Zitnik, J. Shang, C. Langlotz, and J. Han, "Cross-type biomedical named entity recognition with deep multi-task learning," *Bioinformatics*, vol. 35, no. 10, pp. 1745–1752, May 2019.
- [22] S. S. Tozonia, G. F. Dias, G. Bohnena, N. Grobeb, R. Pecoits-Filho, P. Kotankob, and A. N. Moreno-Amarala, "Uremia and hypoxia independently induce eryptosis and erythrocyte redox imbalance," *Cell Physiol. Biochem.*, vol. 53, pp. 794–804, Oct. 2019.
- [23] A. F. Lafala Manzano, A. F. Gil Lorenzo, V. Bocanegra, V. V. Costantino, V. Cacciamani, M. E. Benardon, and P. G. Vallés, "Rab7b participation on the TLR4 (toll-like receptor) endocytic pathway in shiga toxin-associated hemolytic uremic syndrome (HUS)," *Cytokine*, vol. 121, Sep. 2019, Art. no. 154732.
- [24] D. Verzola, S. Milanese, F. Costigliolo, and G. Garibotto, "Immunohistochemical staining of TLR4 in human skeletal muscle samples," *Bio-Protocol*, vol. 9, no. 2, pp. 1–17, 2019.
- [25] P. M. K. Njage, P. Leekitcharoenphon, and T. Hald, "Improving hazard characterization in microbial risk assessment using next generation sequencing data and machine learning: Predicting clinical outcomes in shigatoxigenic escherichia coli," *Int. J. Food Microbiol.*, vol. 292, pp. 72–82, Mar. 2019.
- [26] Á. D. O. Franco, R. T. Starosta, and M. Roriz-Cruz, "The specific impact of uremic toxins upon cognitive domains: A review," *Brazilian J. Nephrol.*, vol. 41, no. 1, pp. 103–111, 2019.



**JING HUANG** was born in Henan, China, in 1982. She received the master's degree from the Tongji Medical College, Huazhong University of Science and Technology, in 2007. She is currently working with the Affiliated Cancer Hospital, Zhengzhou University. Her research interests include multiple organ dysfunction syndrome (MODS) and respiratory failure.

• • •